WP2 PERIODIC REPORT

Grant Agreement number: 250072

Project acronym: ISENSE

Project title: Integrated Quantum Sensors

Funding Scheme: STREP (ICT-FET-Open)

Date of latest version of Annex I against which the assessment will be made: 4. March 2011

Periodic report: 1st ☐ 2nd ☐ 3rd X 4th ☐

Period covered: from 1. July 2012 to 30. June 2013

Name, title and organisation of the scientific representative of the project's coordinator[1]:

Professor Kai Bongs,
College of Engineering and Physical Sciences, School of Physics and Astronomy, University of Birmingham

Tel: +44 121 414 8278

Fax: +44 121 414 8277

E-mail: k.bongs@bham.ac.uk

Project website[2] address: http://www.isense-gravimeter.eu/

---

[1] Usually the contact person of the coordinator as specified in Art. 8.1. of the grant agreement

[2] The home page of the website should contain the generic European flag and the FP7 logo which are available in electronic format at the Europa website (logo of the European flag: http://europa.eu/abc/symbols/emblem/index_en.htm ; logo of the 7th FP: http://ec.europa.eu/research/fp7/index_en.cfm?pg=logos). The area of activity of the project should also be mentioned.

WP 2- *Science Chamber and Scheme*
Work package leader: CNRS-SYRTE

Introduction

The overall objective of this work package is to establish and optimize the technological steps necessary to realize a guided atomic quantum sensor, in which atoms are either trapped in optical lattices or levitate thanks to sequences of laser pulses. The feasibility of this technology for gravity sensing will be demonstrated, a small scale ($<$ 1liter) vacuum chamber and an adapted low power atom chip developed. The work will be carried out keeping two main constraints into account: the physical principle has to operate in a reduced volume, the chosen species for the technology demonstrator is Rb. In addition we will lay the foundations to broaden the iSense platform to include further species, which are in particular interesting as optical time and frequency standards or for quantum information applications. Particular attention will be devoted on the evaluation of performances of interferometric schemes applied on alkali-earth species in comparison with alkali atoms.

The work package is organised by subdivision in four tasks, which are listed in the table below.

Task-Nr.	Task	Task Leader
2.1	Interferometer scheme	CNRS-SYRTE
2.2	Low power atom chip	UNOTT
2.3	Small scale vacuum chamber	CNRS-IOGS
2.4	Alternative atoms and schemes for future sensors	UNIFI

Summary of progress towards objectives

We have selected a scheme developed by ONERA for the iSense sensor during the last reporting period. We have now gained support from ONERA to provide expertise in implementing this scheme.

Noise evaluations have been performed and multi-wave interferometry schemes have been tested.

Progress on trapping, cooling and handling Sr and Yb isotopes as well with Rb-Sr mixtures has been made, demonstrating fermionif Yb degernerate gases and mixed Rb Sr degenerate gases.

Details for each task;

Task 2.1
- *Interferometer Scheme (months 1-24).*

This task has been finished with the selection of an interferometer scheme as discussed in the last report. Monitoring external as well as internal developments we have chosen an external scheme developed by ONERA for the iSense demonstrator, as this promises higher sensitivity as well as flexibility in terms of compatibility with free fall schemes. We have secured scientific support from ONERA in order to ensure efficient implementation of this scheme.

In addition at SYRTE, we have demonstrated a new variant of the Wannier-Stark scheme: a time domain atomic multiwave interferometer. In our experiment, ^{87}Rb atoms trapped in a shallow vertical optical lattice are manipulated using Raman transitions. We apply Raman laser pulses with Rabi frequencies larger than the Bloch frequency ν_B, which corresponds to the energy separation between consecutive wells. These pulses thus coherently drive transitions between multiple Wannier-Stark (WS) states, allowing tunnelling of atoms into several neighbouring sites of the optical lattice. Between two such pulses, atoms are in a superposition of several WS states. Each

WS state is a partial matter wave, which evolves with a phase of $\Phi_m = 2\pi\, m\, \nu_B$ (m is the well index). These waves rephase at every Bloch period, which gives rise to a periodic interference pattern. This multiwave interferometry phenomenon is similar to Bloch oscillations, where Bloch oscillations are interpreted as periodic rephasing of the many WS components of a pure Bloch state. In our multiwave interferometer, Raman transitions are used as a state labelling tool changing both the internal and external state of the atoms, allowing for an efficient detection based on the internal state populations, and not on the external state (position or momentum). This method gives interference fringes without any modulation of the lattice depth. Furthermore, atoms are in the same internal state during the whole interference evolution process, this makes the interferometric phase insensitive to light shifts induced by the trapping and Raman lasers.
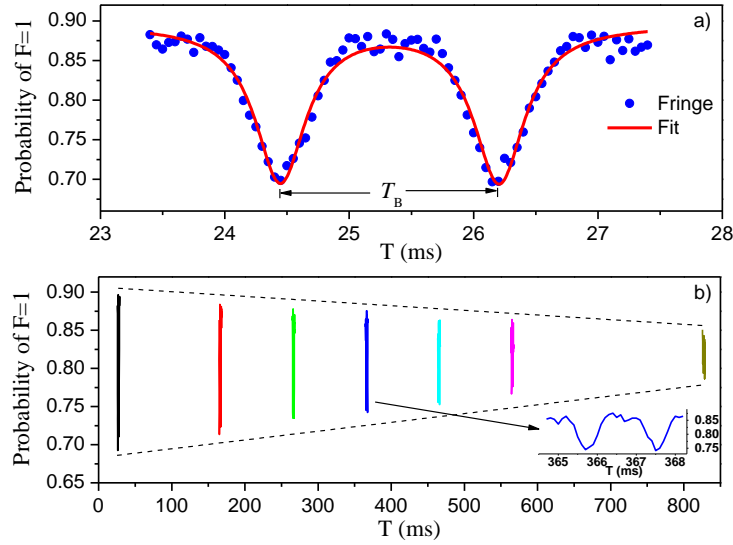
Fig. 2.1: Multiwave atom interferometer fringes.

From the period of the fringes, we derive the Bloch frequency with a relative sensitivity of $1.5\ 10^{-4}$ at 1s. This is one order of magnitude less sensitive than the Ramsey type interferometers we have demonstrated previously. The sensitivity is detection noise limited. With respect to the Ramsey interferometer, the number of detected atoms is greatly reduced by the selection after the first Raman pulse: typically 80% of the atoms remaining in F=2 are blown away by the pusher pulse.

UNIFI carried out an experimental investigation of the main sources of noise and systematic errors in differential gravity measurements with Rb Raman interferometry down to the 10^{-11} g level. In particular, we studied the influence of most relevant experimental parameters (DC and transient magnetic fields, frequency and intensity of cooling, repumping, Raman and probe laser beams, as well as alignment of Raman laser beams) on noise and biases. After active control of the most critical parameters, we achieve a short term sensitivity of 3×10^{-9} g/√Hz to differential gravity acceleration, and a resolution of 5×10^{-11} g after 8000 s.

One challenge in order to attain extreme performances in atom interferometry gravitational measurements is to carefully control the external degrees of freedom of the atomic probe. We analysed the influence of the position and velocity of the atoms in an atomic fountain on the precision of gravity gradient measurement by atom interferometry.

The differential interferometric phase depends on the position and velocity of the two atomic clouds mainly through four effects: gravity gradients, rotations, wavefront curvature of Raman beams, and magnetic gradients. In the following we'll discuss the first two contributions.

As long as the atoms are launched with some residual horizontal velocity along the East-West direction, the Coriolis force yields a phase shift on the atom interferometer output. The ellipse phase shift φ_{Coriol} due to Coriolis effect is proportional to the velocity difference Δv_{E-W} between the two clouds along the East-West direction.

In the UNIFI experiment the two clouds are launched to about 60 and 90 cm above the MOT position, and the launching velocities are $v_l \simeq 3.5$ m/s and $v_u \simeq 4.3$ m/s for the lower and upper cloud respectively. If both clouds are launched with the same tilt angle θ_{tilt} along the E-W direction, their horizontal E-W velocities will differ by about 25% from each other, and the resulting Coriolis shift will be $\varphi_{Coriol} \simeq -34\ \theta_{tilt}$.

The effect of Coriolis force on the atom interferometer can be mitigated by counter-rotating the retro-reflection mirror for the Raman beams during the measurement. We apply a linear rotation ramp to a tip-tilt mirror in order to keep the direction of the effective k-vector parallel during the measurement. This is achieved when the mirror rotation is exactly opposite to the Earth rotation. The effect of the tip-tilt is shown in figure 2 where the RMS error of ellipse fitting is plotted versus the mirror rotation rate along the E-W direction. Mirror rotation increases the ellipse error both by decreasing the contrast, due to limited overlap of the wave-packet at the interferometer output, and by increasing the Coriolis-induced phase scatter due to the distribution of transverse velocities.
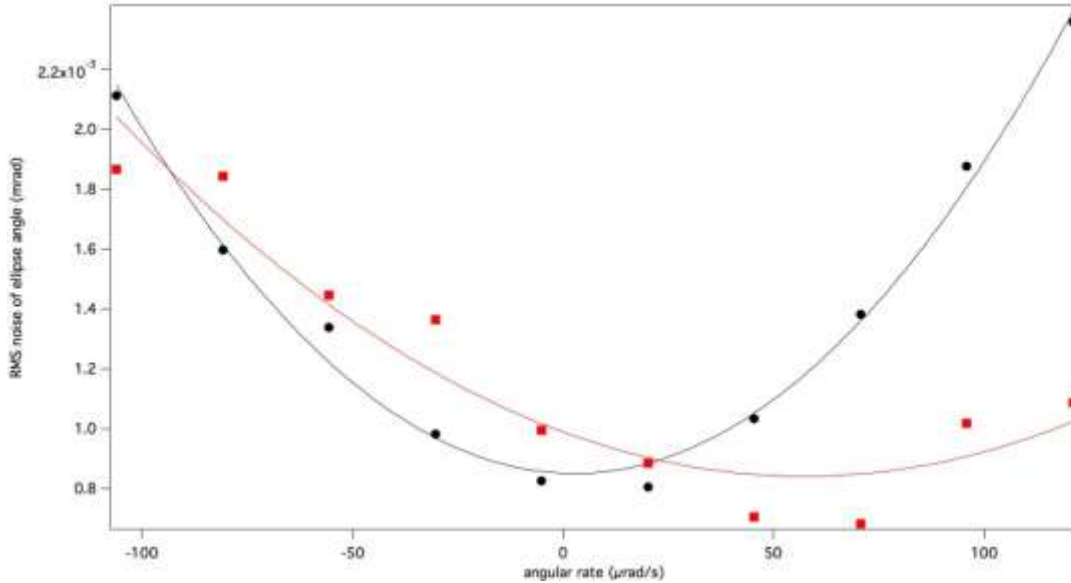
Fig. 1.2: RMS error of ellipse fitting versus tip-tilt rotation rate along the East-West (red) and North-South (black) direction. Full lines are parabolic fittings to experimental data. The minimum corresponds to 57±3 μrad/s for E-W, and to 2±3 μrad/s for N-S

The minimum noise corresponds to the condition in which the Earth rotation is best compensated. We determine the optimal rotation rate with a precision of 5%, thus we reduce the Coriolis effect by a factor 20 at least.

We reverse the logic of this method and employ the Coriolis shift in order to characterize the transverse atomic velocities. The Coriolis induced phase shift in the atom interferometer is proportional to the transverse average velocity of the atoms along the rotation direction, to the

4

rotation rate of the mirror, to the effective k-vector and to the square of the interferometer time T. By recording the interferometer phase versus the applied rotation rate of the tip-tilt mirror, we determine the linear coefficient which is proportional to the transverse velocity. With our current sensitivity on φ, we currently determine the transverse atomic velocity with a resolution of ~5 μm/s.

Besides the effects of trajectory fluctuations, other possible sources of systematic shift are given by gravity gradients. In our setup, the geometry of source masses is chosen in such a way that the gravitational potential is stationary in the region of the atom interferometry measurement, i.e. at the apogees of atomic trajectories. The curvature of gravitational potential is larger in the horizontal plane than in the vertical direction. In the case of point-like atomic clouds with a common traverse displacement from the symmetry axis of source masses, the differential interferometric phase varies by 42 μrad/mm2 around the axis. Accurate measurements with the atom interferometer require a precise knowledge of the density distribution in the atom clouds.

For the knowledge of vertical positions and velocities we employed time of flight (TOF) measurements. We determined the time t_a at which the velocity selected atoms reach the trajectory apogee, i.e. when $v_z = 0$. Such condition can be easily identified using a Raman π transition: if atoms are at rest roughly half of them undergo the Raman transition with a positive momentum recoil, while the remaining fraction will have a negative momentum recoil. As a consequence the detected signal shows two symmetrical peaks. Then we measure the time t_d at which the atoms cross the detection region. From the knowledge of the vertical position z_0 of the detection light sheet we can deduce the height z of the apogee. We also measured the transverse position of MOT and tilt angles of the two clouds in the atomic fountain with respect to the Raman beams propagation direction. We carefully aligned the Raman beams along the symmetry axis of the source masses. We used the Raman beam pair itself as a reference to probe the atomic samples.

We measured the horizontal distribution of atomic clouds at different heights in the ballistic flight of the fountain. We employed the Raman laser beams to define a reference frame for the atomic positions. A portion of radius $r \simeq 4$mm of the downward-propagating Raman beam was selected with a diaphragm mounted on a 2D translation stage. We addressed the atoms with three Raman pulses in rapid sequence, and finally detected the number of atoms in F = 1. We probed the horizontal distribution of atomic density in both clouds simultaneously by scanning the position of the diaphragm. The number of detected atoms is proportional to the atomic density in the column selected by the diaphragm and to the transition probability of Raman beams. We deduced the distribution of transition probability from the intensity profile of Raman beams and from the direct measurement of transition probability versus Raman power. Typical reconstructed density profiles in the transverse direction are shown in figure 3 for the two clouds and for different times of ballistic flight. We achieved a resolution better than ~0.1 mm in the determination of both the cloud centre and its width.
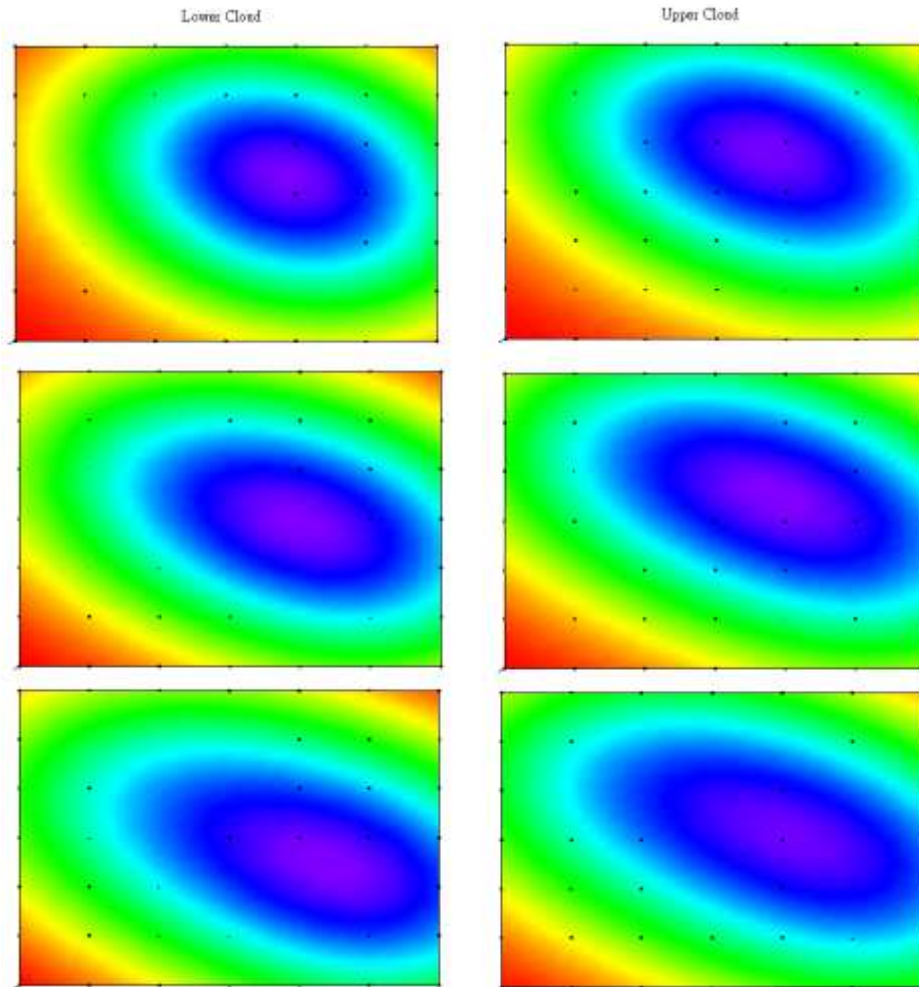
Fig. 2.2: Reconstructed profile of the density distribution of lower cloud (left) and upper cloud (right), at different times after launch.

Task 2.2
- ***Test of novel transparent materials (months 24-48).***

This task has not yet been started, as external experiments have demonstrated the feasibility of transparent materials in general making it more appropriate to focus fabrication resources on the integrated optics system.

Task 2.4
- ***Experimental test of alternative interferometric schemes on Sr and Yb and estimation of potential sensitivity of the sensor. (month 24-48)***

- ***Assess of possible new schemes based on the application of quantum degenerate gases and control of collisional parameter (K, Sr) with the aim to reach sensitivities better than 1 µgal/Hz^1/2. (LUH, IQOQI-OEAW, month 24-48)***

Following the achievement of Bose-Einstein condensation of ^{174}Yb at Hamburg in June 2012, we have retrofitted the cooling and trapping laser systems to improve their performance and stability further, e.g. by optimising the loading volume of dipole trap to transfer up to 1.2×10^7 from the 3D-

MOT. Due to these modifications, we routinely produce nearly pure BECs of 2×10^5 ^{174}Yb atoms, while cycle durations of down to eight seconds may be used thanks to an improved loading rate of the 3D-MOT of more than 1.5×10^7 s^{-1}. Subsequently, we have implemented and optimised 2D- and 3D-magneto-optical trapping of the spin-5/2 fermionic isotope ^{173}Yb as well as evaporative cooling in the crossed optical dipole trap. Degenerate Fermi gases of more than 2×10^4 atoms at temperatures as low as $T/T_F = 0.15$ are routinely produced in our apparatus.
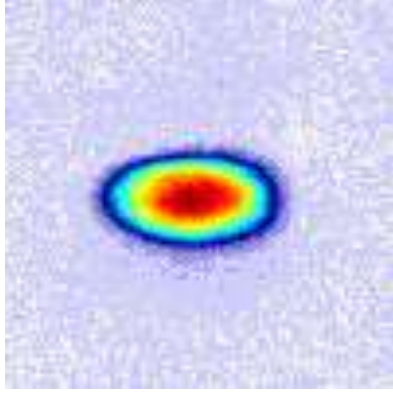
Fig. 2.4: Nearly pure BEC of Yb-174
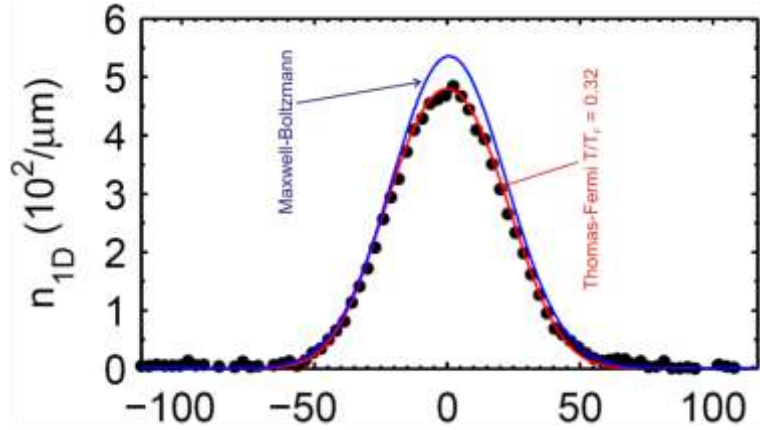
Fig.2.5: Profile of a degenerate Fermi gas towards the end of evaporative cooling.

In parallel to these efforts, we have improved the clock laser system for spectroscopy on the ultranarrow $^1S_0$-$^3P_0$ transition. Temperature stabilisation and isolation of the ultrastable resonators from mechanical vibrations have been implemented, and laser locking with subhertz linewidths has been achieved. Linewidths of currently about 5 Hz have been observed between two lasers locked to different ultrastable resonators, indicating that the performance of the clock laser is more than sufficient for precision spectroscopy of the $^1S_0$-$^3P_0$ transition.

In the past months, we have used the clock laser system to perform preliminary precision spectroscopy of ultracold fermionic samples in a one-dimensional optical lattice at the magic wavelength, which has been set up for this purpose. Spectra with linewidths of several kilohertz have been observed in this lattice, and we recently added a triangular lattice at the magic wavelength in the perpendicular plane in order to improve on these results. We are confident that in a 3D optical lattice we will be able to perform precision spectroscopy at much lower linewidths and use it to coherently prepare and manipulate quantum-degenerate samples of ^{173}Yb and ^{174}Yb.
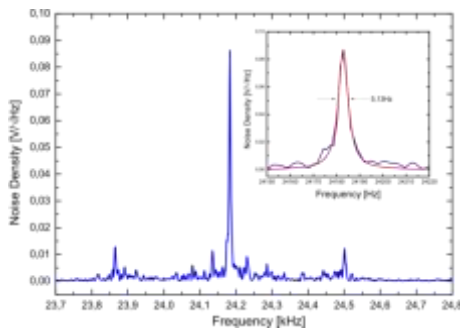
Fig.2.6: Beat signal of lasers stabilised to the two ultrastable optical resonators.
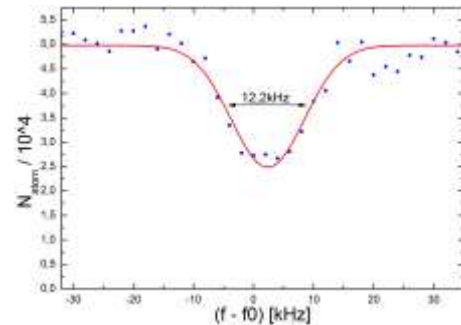
Fig.2.7: Spectroscopy scan across the clock transition of Yb-173 along a one-dimensional optical lattice.

At IQOQI, we have performed sympathetic laser cooling of Rb by Sr. A sample of Rb contained in a dipole trap is sympathetically cooled by Sr that is laser cooled on a narrow-linewidth transition. The phase-space density of the Rb sample is increased by a factor 250 in less than 400ms, reaching 0.05. The ability to create a high phase-space density Rb sample in a very short time, can be very valuable for future atom interferometers. A Rb-Sr double Bose-Einstein condensate was also realized, and we have determined the Rb-Sr interspecies scattering properties by two-color photoassociation. The knowledge of the interspecies scattering properties allows to optimise sympathetic laser cooling of Rb by Sr.

IOGS optimized the non-destructive detection system based on a heterodyne detection to measure the number difference between the two hyperfine states of rubidium atoms. The probing method has been used in a feedback loop to control the internal states of trapped coherent ensembles of two-level atoms, and to protect a superposition state against the decoherence induced by a collective noise. The feedback control is based on weak optical measurements with negligible backaction followed by coherent microwave manipulations. We studied the efficiency of the feedback system for a simple binary noise model and characterized in terms of the trade-off between information retrieval and destructivity from the optical probe. We also demonstrated the correction of more general types of collective noise, namely binary collective rotations repeated several times, and analog collective rotations. We are actually using the technique to operate an atomic interferometer beyond the standard Ramsey scheme, so as to obtain a longer effective interrogation time and hence precision in a microwave clock.

UNIFI completed the analysis of a multiwave interferometer with trapped ^{88}Sr atoms in optical lattices. Observation of Bloch oscillations is improved with the application of coherent delocalization by means of resonant lattice modulation prior to evolution in the static lattice. However, acceleration sensitivity with DEBO (Delocalization-Induced Bloch Oscillations) is limited by experimental drift due to position fluctuations of the red MOT, which critically depends on bias magnetic fields. On the other hand, the observation of resonant frequency in the spectrum of sample size vs lattice AM provides a determination of the Bloch frequency, and thus of the axial acceleration, which is limited by MOT size instabilities. The long term resolution in gravity measurement is found to be $\sim 10^{-6}$ g with DEBO and 1.5×10^{-7} g with AM. We also observed the occurrence of decoherence mechanisms when measuring in the proximity of a transparent surface, and verified that the scaling of decoherence versus distance is compatible with Rayleigh scattering of the lattice laser beams from the surface.

We performed a preliminary, sequential measurement of differential gravity acceleration with two different Sr isotopes; the differential measurement will provide a tool for the investigation of ultimate sources of noise and systematic errors, as well as a test of the weak equivalence principle for particles with different statistics. We load about 8×10^6 ^{88}Sr atoms and about 5×10^5 ^{87}Sr atoms in the vertical optical lattice (see figure)
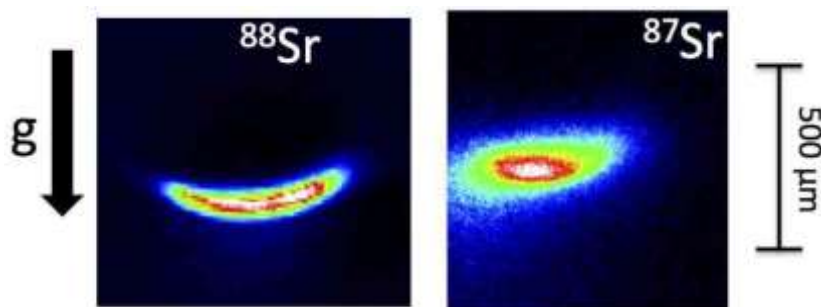
Fig. 2.8: absorption images of red MOT for the two Sr isotopes

Clearly significant results

We are further investigating the iSense schemes and have developed a new variant of the Wannier-Stark scheme at SYRTE.

The Yb apparatus in UHH was improved to also produce degenerate fermionic samples and now offers a Hz linewidth clock laser for precision measurement tasks.

A Sr-Rb double degenerate gas was produced at OEAW-IQOQI and a non-destructive scheme to assess the hyperfine population in Rb was developed and demonstrated to provide improved Ramsey interferometry.

Noise effects in free fall gravity gradient atom interferometry have been investigated in Florence and advanced schemes based on Bloch oscillations have been characterized.

Deviations from Annex I and their impact on other tasks, available resources and planning
NA

Reasons for failing to achieve critical objectives and/or not being on schedule and explain the impact on other tasks as well as on available resources
.

Statement on the use of resources, highlighting and explaining deviations between actual and planned person-months per work package and per beneficiary in Annex 1
The use of resources is in general agreement with Annex-I.